

THE OPTICAL-UV CONTINUUM OF A SAMPLE OF QSOs

F. Natali¹, E. Giallongo

Osservatorio Astronomico di Roma, via dell'Osservatorio, I-00040, Monteporzio, Italy

S. Cristiani

Dipartimento di Astronomia Università di Padova, vicolo dell'Osservatorio 5, I-35122 Padova, Italy

and

F. La Franca

Dipartimento di Fisica - Università degli studi "Roma Tre", via della Vasca Navale 84, I-00146 Roma, Italy

ABSTRACT

The average optical-UV continuum shape of QSOs has been investigated using spectra of 62 QSOs having good relative photometric calibrations. The QSO spectra were extracted from two complete color selected samples in the magnitude intervals $B \approx 16-20$. The analysis was performed fitting power-law continua $f_\nu \propto \nu^\alpha$ in well defined rest-frame wavelength intervals after removing regions of the spectrum affected by strong emission lines or weak emission bumps. The average slope in the rest-frame optical-UV region $1200 - 5500 \text{ \AA}$ shows a rapid change around the 3000 \AA emission bump with $\alpha \simeq 0.15$ longward of it and $\alpha \simeq -0.65$ at shorter wavelengths. Although these average slopes have been obtained using spectra of QSOs with different luminosities and redshifts, there are no significant correlations of the average spectral index with these quantities. For a few QSOs in the sample we were able to measure the same softening of the spectral shape within the individual spectrum. These results have significant consequences on the estimate of the cosmological evolution of the optically selected QSOs as they affect, for instance, the k -corrections. New k -corrections in the B, V, R and Gr bands were computed. The derived average spectral shape in the optical-UV band puts interesting constraints on the expected emission mechanisms.

¹Istituto Astronomico - Università "La Sapienza" di Roma, Via Lancisi 29, I-00161 Roma, Italy

1. Introduction

The study of the shape of the QSO continuum has a great importance both for the identification of the emission mechanisms responsible for the observed radiation and for the estimate of the QSO cosmological evolution.

The continuum spectrum is conventionally parameterized in the optical-UV region by a power law of the type $f_\nu \propto \nu^\alpha$. This is a local approximation: in the recent years the availability of IR, UV and X-ray data has allowed to measure the energy distribution of QSOs in a wide spectral range, showing large deviations from a single power-law approximation. Even in the optical-UV region, composite spectra derived from complete color selected samples (Cristiani & Vio 1990, Francis et al. 1991) show significant departures from a single power-law.

Another remarkable occurrence is the variety of results obtained in the many studies of the shape of the optical-UV continuum spectrum, in particular about the estimated average optical-UV spectral index, α , and its dispersion. Roughly the intrinsic optical-UV spectral index ranges from -1 to 0. O'Brien et al. (1988) and Sargent et al. (1989) obtain $-0.7 \leq \alpha \leq -0.6$ on two large samples; Oke & Korycansky (1982), Oke et al. (1984), Baldwin et al. (1989) and Cheng et al. (1991), found values in the range $-1 \leq \alpha \leq -0.5$ from smaller samples. Recently some studies found an intrinsic spectral index $\alpha \sim -0.3$ (Sanders et al. 1989, Francis et al. 1991, Webster et al. 1995, Francis 1996), in agreement with the expected slope provided by free-free emission models (Barvainis 1993).

However, most of the differences among the results quoted in the literature might be due to the different spectral intervals used to estimate the average continuum slope.

No substantial agreement exists also about the dispersion of the observed spectral index, σ_α , and its origin: obscuring dust (Webster et al. 1995), intrinsic differences in the spectral energy distribution from QSO to QSO (Sargent et al. 1989, Serjeant & Rawlings 1996), or simply measurement errors (Cheng et al. 1991). Some authors claim no intrinsic dispersion (Sanders et al. 1989), others state a large one (Elvis et al. 1994): so far the observed values of the dispersion range from 0.2 to 0.5.

Determining the average shape of the optical-UV emission and whether it is intrinsically the same for

all the QSOs is not a worthless question. The choice of $\alpha = -0.7$ rather than -0.3 to calculate the k -corrections leads to increase the luminosities of QSOs at $z \simeq 2$ of a factor ≈ 2 . An appreciable dispersion ($\sigma = 0.3$), as well, introduces uncertainties in the luminosity and biases the estimate of the cosmological evolution of the luminosity function (Giallongo & Vagnetti 1992, Francis 1993, La Franca & Cristiani 1997).

In this paper we present a spectroscopic study of a set of 62 objects extracted from a complete sample of radio-quiet QSOs. We determine the values of the mean spectral index in four different ranges of rest frame wavelength, with a particular attention to the correlations between α and the redshift or the luminosity.

We describe in Sect. 2 the data set and in Sect. 3 the method we used to perform the power law fit to the continuum. Finally, in Sect. 4, we show the observed dependence of the spectral index on the mean rest frame wavelength and present new k -corrections to estimate the evolution of the QSO luminosity function (LF).

2. Data sample

The QSOs studied in the present work belong to the Selected Area 94 (La Franca et al. 1992; $m_B \leq 19.9$) and the Homogeneous Bright Quasar Survey (HBQS, Cristiani et al. 1995; $15 \leq m_B \leq 18.75$). Both samples identified quasar candidates on the basis of UV criteria (complementary objective-prism data have been also used in a few subareas to cross check the effectiveness of the selection). From this sample a subset of 62 QSOs was extracted with a good relative photometric calibration and with a luminosity and redshift distribution similar to the original set (Figure 1). It is to notice that the spectral properties of our sample are representative of QSOs selected with an UV excess and a bias against radio-loud quasars showing very red colors can be present (Webster et al. 1995, Francis 1996). On the other hand it is not known at present if radio-quiet dust-reddened objects represent a considerable fraction of the QSO population.

The observations of the QSOs have been carried out at the 3.6m, 2.2m ESO/MPI and 1.5m ESO telescopes at La Silla, equipped either with the ESO Faint Object Spectrograph and Camera (EFOSC1 - EFOSC2), or with the Boller and Chivens Spectro-

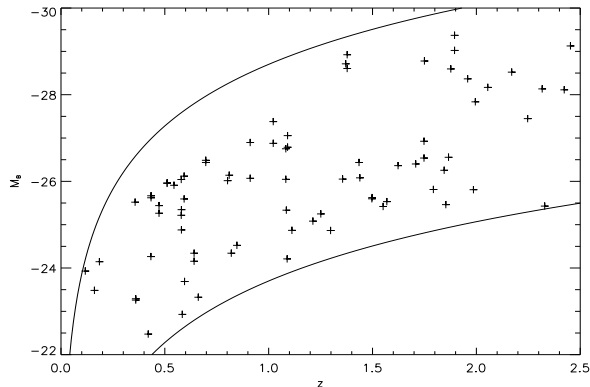


Fig. 1.— Luminosity *vs* redshift plot of the QSO sub-sample studied. The apparent magnitude loci at $m_B = 15$ and $m_B = 20$ are shown ($h_0 = 50$; $q_0 = 0.5$).

graphs. The slit had typically a width at least 1.5 times the seeing FWHM and in general was placed at the parallactic angle. The detectors were always CCDs. The resolution of the spectra ranged between 10 and 30 Å. The reduction process used the standard MIDAS facilities (Banse et al. 1983) available at the Padova Department of Astronomy and at ESO Garching.

The raw data were sky-subtracted and corrected for pixel-to-pixel sensitivity variations by division by a suitably normalized exposure of the spectrum of an incandescent source. Wavelength calibration was carried out by comparison with exposures of He-Ar, He, Ar and Ne lamps. Relative flux calibration was finally achieved by observations of standard stars listed by Oke 1974 and Stone 1977. The airmass of the observation was always below 1.6 and has been corrected on the basis of the standard La Silla extinction tables.

3. Fitting the continuum

As discussed in the previous sections the shape of the continuum component of the QSO spectra changes considerably over different frequency bands.

In the optical-UV band the continuum is usually parametrized as a power law: $f_\nu \propto \nu^\alpha$. Some results (Cristiani & Vio 1990, Francis et al. 1991) show that, even in the optical-UV range (1200-10000 Å), the continuum spectrum of individual QSOs is not well represented by a single power law (i.e. $\alpha = \text{constant}$ over the whole band). However these results are obtained

with the technique of the composite spectra, based on the simplifying assumption that each spectrum is representative of the whole QSO “class” and an ensemble mean can be meaningfully applied. Such an hypothesis may result too simplistic and even misleading: it is well known, for example, that the average of a number of power-laws of different spectral index is not a single power-law.

In this study we have estimated the *local* power-law shape of the individual QSOs in four ranges, namely the rest-frame intervals: 1400 – 2200 Å, 2150 – 3200 Å, 2950 – 4300 Å, 3900 – 5500 Å. Some spectra of the extracted set of QSOs cover a large frequency range, so in few cases we have, for the same QSO, two different rest-frame wavelength intervals. We have obtained 78 spectral ranges from the extracted set of 62 QSOs.

For each spectral range the regions certainly contaminated by strong emission were eliminated and an automatic algorithm was applied to estimate the power law index α over the spectral regions described above. The number of available regions in individual QSO spectra depends on the redshift and on the instrumental response of the spectrographs used.

The method consists in a first selection of the probable *continuum window* regions within each spectral interval. These continuum windows are selected on the basis of the composite emission line spectra published by Cristiani & Vio (1990) and Francis et al. (1991).

The local power-law continuum is determined by a linear regression on the local minima of the spectrum selected after appropriate smoothing to improve the S/N ratio. Each minimum is weighted by the reciprocal of the local second derivative of the spectrum, to minimize the effects of occasional absorptions. The weight is doubled for those local minima which, following the results on the composite spectra, are within identified *continuum windows* (see Table 1).

4. Results

4.1. Continuum slope

The mean value of the spectral index, $\overline{\alpha}$, averaged over the whole sample, is -0.33 with a root mean square dispersion of 0.59, in agreement with the value found by Francis (1993) for the Large Bright Quasar Survey (LBQS). This value of the dispersion, however,

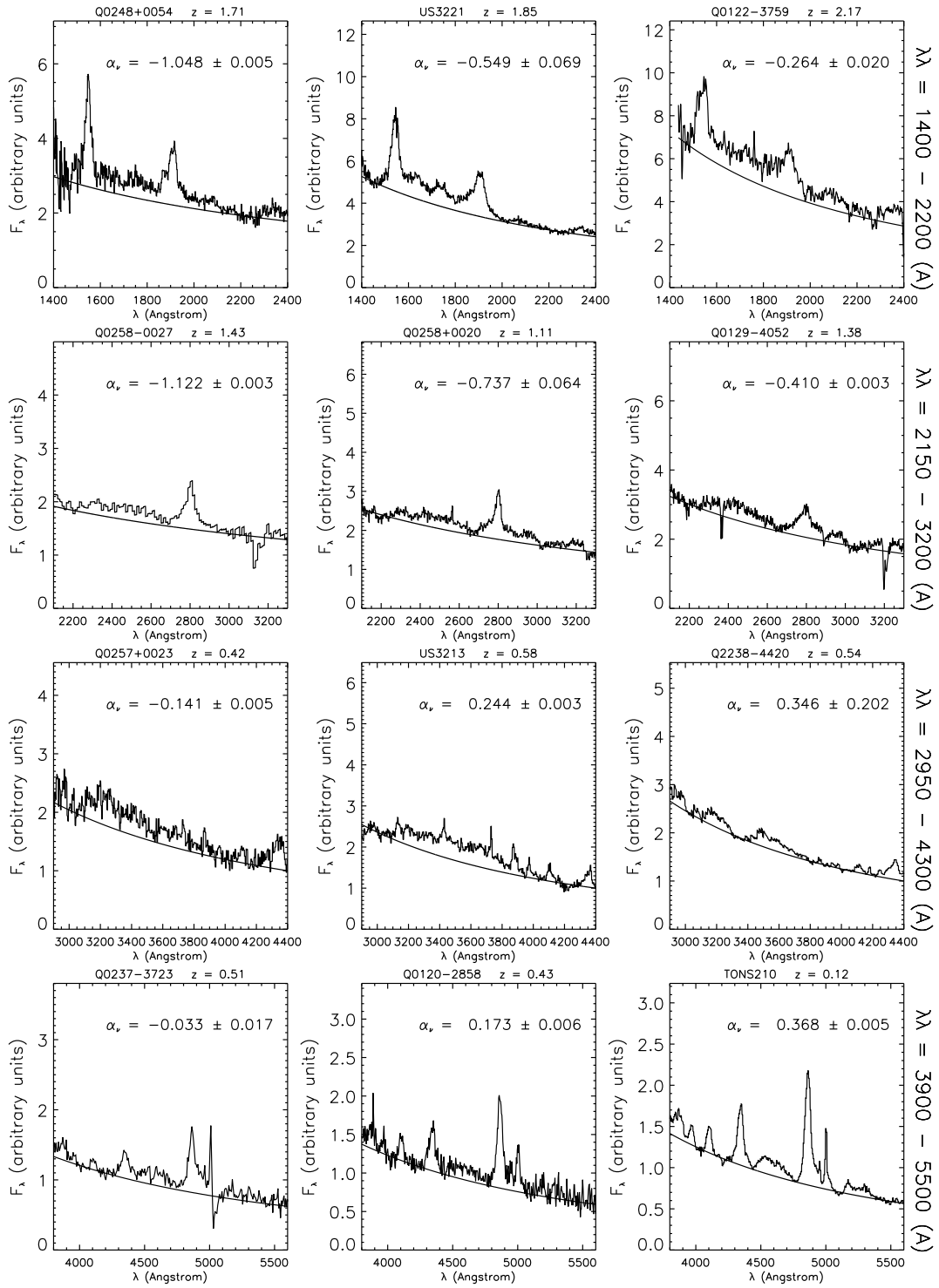


Fig. 2.— Examples of QSOs' spectra with fitted continuum and resulting spectral index in the given rest wavelength interval.

although supported by Elvis et al. (1994), is significantly higher than that (≈ 0.3) found by Sanders et al. (1989) and recently by Francis (1996). If the power-law index is a function of the wavelength, the different results can be understood in terms of measurements in different rest-frame spectral regions: indeed, under the hypothesis of significant deviations from a single power law, we do expect a large dispersion over the whole sample.

The mean values of the continuum slopes obtained for each of the four rest wavelength intervals described above are reported in Table 1 together with their dispersions. For 7 QSOs it was possible to fit the continuum only in the range 1700 – 2700 Å. Figure 3 shows the dependence of the spectral index from the mean rest wavelength of the fitted spectrum: noticeable the presence of a break in the values from $\overline{\alpha}_\nu \simeq -0.65$ to $\overline{\alpha}_\nu \simeq 0.15$ at $\bar{\lambda} \simeq 3200$ Å. In this case the dispersions are lower (see Table 1) than found for the whole sample.

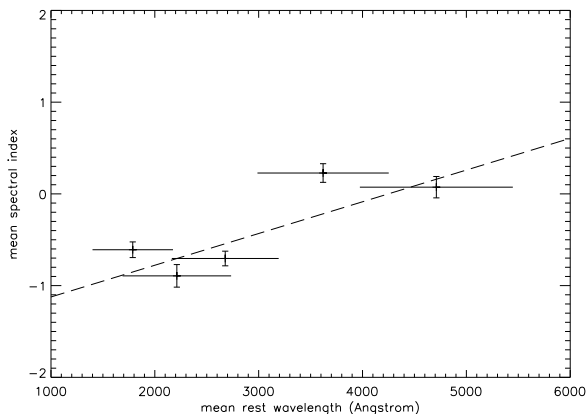


Fig. 3.— Dependence of the mean spectral index from the mean rest wavelength of the fitted spectrum. Along the y-axis are plotted the errors in $\overline{\alpha}_\nu$, while along the x-axis the average baseline of the fit is shown for each rest wavelength interval.

To represent the overall shape of the average QSO continuum as a gradual change of the local slope as a function of wavelength we have assumed a linear trend of α_ν vs $\bar{\lambda}_{rest}$ (Figure 3), i.e. $\overline{\alpha}_\nu = a(\frac{\bar{\lambda}}{4400}) + b$ (where the wavelength is expressed in Angstrom); we derived $a = 1.5 \pm 0.3$ and $b = -1.5 \pm 0.2$ by a linear fit with errors in both coordinates (see Fasano & Vio 1988). In this case, because of $\alpha_\nu = \frac{dLogF_\nu}{dLog\nu}$, the optical-UV continuum is expressed by a more complicated

function of the wavelength:

$$LogF_\nu = \left(b - \frac{k}{\nu Log\nu} \right) Log\nu \quad (1)$$

where $k = \frac{a}{4400 \ln 10} c$ (c is the speed of light).

No significant correlation between α_ν and the redshift or the luminosity was found (Table 2), in agreement with the results obtained by Richstone & Schmidt (1980), Oke et al. (1984) and Cheng et al. (1991). In all the four wavelength ranges we have $|\frac{d\alpha_\nu}{dz}| < 0.4 \pm 0.4$ and $|\frac{d\alpha_\nu}{dM_B}| < 0.1 \pm 0.1$, with a probability greater than 15% of no correlation between α_ν and redshift or luminosity. Since $\overline{\alpha}_\nu$ has been found roughly constant below and above 3200 Å, we studied the correlation with z and M_B in the two larger wavelength intervals 1400 – 3200 Å and 3200 – 5500 Å (Figure 4), combining the values of α found in each of the intervals reported in Table 1: even in this case no significant correlation was found.

To avoid spurious results due to the luminosity-redshift correlation present, to some degree, in flux-limited QSO samples, we repeated the correlation analysis in restricted intervals of luminosity and redshift. The mean values of α_ν and their degree of correlation with z and M_B do not change substantially if we choose objects of the sample having luminosities or redshifts in the following intervals: $-27.5 \leq M_B \leq -25.5$, $0.5 \leq z \leq 1.1$. These results suggest that the variations of the spectral index with $\bar{\lambda}_{rest}$ are intrinsic and do not depend on the distribution of QSOs in the redshift-luminosity plane.

As a further check for thirteen objects it was possible to measure the change in the average continuum slope around 3000 Å by fitting the individual continua over two different (contiguous) wavelength baselines: five QSOs over $\lambda\lambda 2150 - 3200$ Å and $\lambda\lambda 2950 - 4300$ Å, eight over $\lambda\lambda 2950 - 4300$ Å and $\lambda\lambda 3900 - 5550$ Å. The resulting mean difference in the spectral indices between the two spectral intervals, averaged over each of the two sets of QSOs, are, in both cases, close to the difference in the values of the mean spectral indices found for the whole sample.

rest wavelength interval	continuum windows	$\bar{\alpha}_\nu$	σ	number of QSOs
1400-2200 Å	1420-1480 Å 2150-2300 Å	-0.61	0.37	19
1700-2700 Å	2150-2300 Å 2600-2700 Å	-0.89	0.32	7
2150-3200 Å	2150-2300 Å 2600-2700 Å 2950-3100 Å	-0.70	0.35	19
2950-4300 Å	2950-3100 Å 3900-4300 Å	0.23	0.48	22
3900-5500 Å	3900-4300 Å 5400-5500 Å	0.07	0.39	11

Table 1: Mean values and dispersions of the continuum slopes obtained for each of the four rest wavelength intervals in which the variations of the spectral index α are within the errors of the fit; also the result for the interval 1700 – 2700 Å (7 QSOs) is shown. In the second column are reported the *continuum window* regions (identified following the results on the composite spectra) falling in each rest wavelength interval.

rest wavelength interval	1400-2200 Å	1700-2700 Å	2150-3200 Å	2950-4300 Å	3900-5500Å
$\frac{d\alpha_\nu}{dz}$	0.43 ± 0.36	—	-0.11 ± 0.27	0.42 ± 0.47	0.30 ± 0.63
$r_{\alpha,z}$	0.277	—	0.101	0.199	0.158
$P(r_{\alpha,z})$	0.25	—	0.68	0.37	0.64
$\frac{d\alpha_\nu}{dM_B}$	0.07 ± 0.07	—	-0.02 ± 0.06	-0.07 ± 0.08	-0.06 ± 0.11
r_{α,M_B}	0.246	—	0.069	0.181	0.171
$P(r_{\alpha,M_B})$	0.31	—	0.78	0.42	0.61
$\frac{d\alpha_\nu}{dz}$		0.11 ± 0.12		0.45 ± 0.33	
$r_{\alpha,z}$		0.146		0.239	
$P(r_{\alpha,z})$		0.34		0.18	
$\frac{d\alpha_\nu}{dM_B}$		-0.00 ± 0.04		-0.07 ± 0.06	
r_{α,M_B}		0.013		0.187	
$P(r_{\alpha,M_B})$		0.93		0.30	

Table 2: Correlation between the spectral index α_ν and both the redshift and the luminosity; r is the correlation coefficient and $P(r)$ is the probability of no correlation. The absolute magnitude was calculated assuming $h_0 = 50$ and $q_0 = 0.5$.

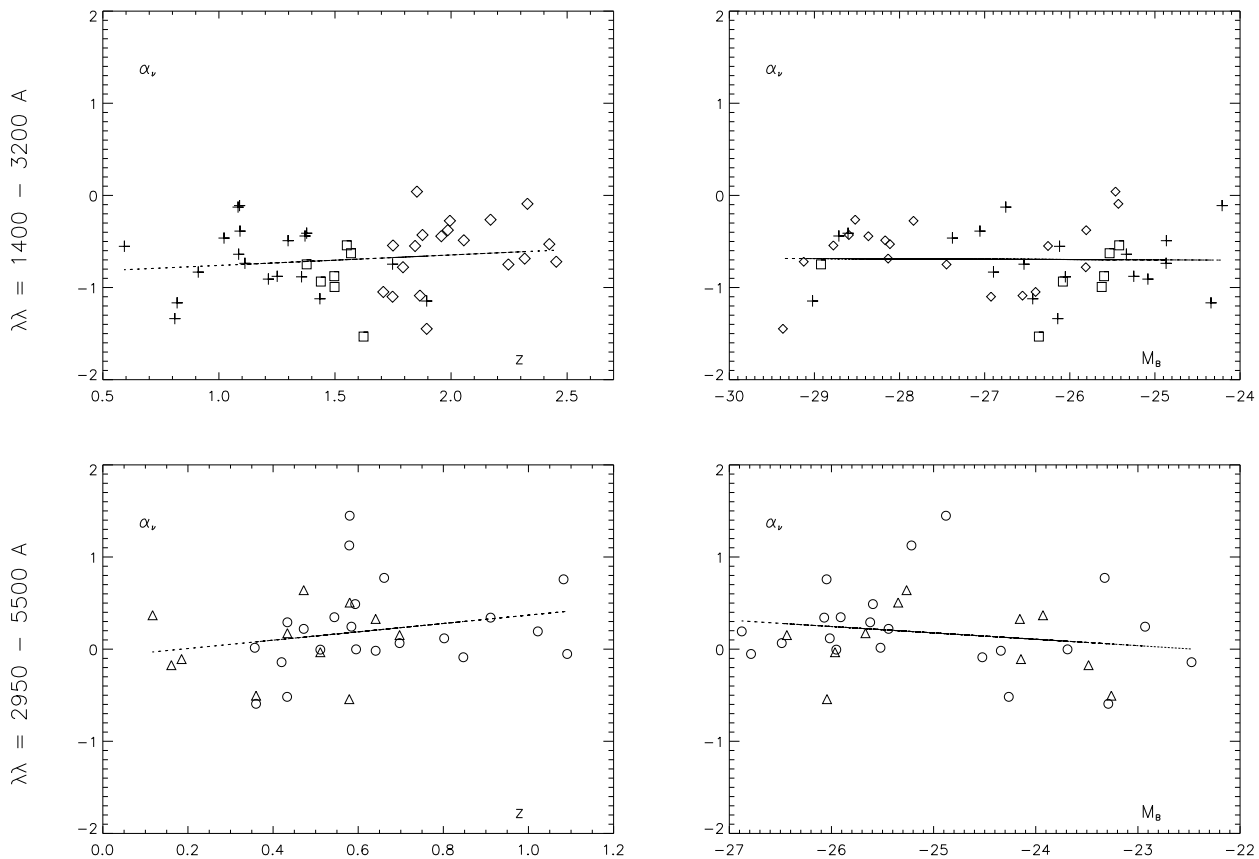


Fig. 4.— Correlation between the spectral index and both the redshift (*left*) and the luminosity (*right*). Different symbols indicate values of α belonging to different rest-frame intervals: 1400 – 2200 (*diamond*); 1700 – 2700 (*square*); 2150 – 3200 (*cross*); 2950 – 4300 (*circles*); 3900 – 5500 (*triangles*). Here is assumed $h_0 = 50$ and $q_0 = 0.5$.

4.2. k -corrections and the evolution of the QSO luminosity function

The shape of the continuum spectrum has an important role in determining the k -corrections and therefore the luminosity function of the QSOs. In fact, because of the different redshifts of the observed objects, to evaluate properly the QSO monochromatic luminosity function and its evolution, the observed flux of the QSOs has to be corrected by a quantity, the k -correction, that depends on the shape of the spectrum.

The k -correction is given by the usual formula

$$k = 2.5 \log(1+z) + 2.5 \log \frac{\int_0^\infty F(\lambda) s(\lambda) d\lambda}{\int_0^\infty F(\frac{\lambda}{1+z}) s(\lambda) d\lambda} \quad (2)$$

K -corrections in the Johnson's B, V, R and Gunn's Gr bands (Table 3) were calculated using equation (2) with a *composite spectrum* (Figure 7) built as follows: we computed the continuum spectrum from equation (1) and the emission component averaging the residuals, respect to their own continuum, of each spectrum of the sample. The k -corrections in the blue bandpass were compared (Figure 5) with the ones derived from two composite spectra having a power law continuum with constant spectral indexes, respectively $\alpha = -0.3$ and $\alpha = -0.5$ and with the k -corrections given by Cristiani & Vio (1990).

z	k_B	k_V	k_R	k_{Gr}
0.1	-0.087	-0.144	-0.036	0.133
0.2	-0.179	-0.234	-0.125	0.242
0.3	-0.232	-0.289	-0.215	0.051
0.4	-0.298	-0.367	-0.281	-0.084
0.5	-0.348	-0.443	-0.342	-0.118
0.6	-0.391	-0.490	-0.408	-0.146
0.7	-0.420	-0.522	-0.471	-0.202
0.8	-0.425	-0.589	-0.520	-0.286
0.9	-0.434	-0.623	-0.549	-0.350
1.0	-0.455	-0.661	-0.600	-0.384
1.1	-0.506	-0.689	-0.646	-0.390
1.2	-0.529	-0.697	-0.672	-0.409
1.3	-0.542	-0.698	-0.703	-0.478
1.4	-0.554	-0.711	-0.727	-0.532
1.5	-0.581	-0.726	-0.740	-0.545
1.6	-0.610	-0.777	-0.743	-0.549
1.7	-0.604	-0.811	-0.752	-0.561
1.8	-0.600	-0.829	-0.761	-0.569
1.9	-0.591	-0.839	-0.780	-0.559
2.0	-0.581	-0.848	-0.819	-0.552
2.1	-0.585	-0.862	-0.838	-0.563
2.2	-0.630	-0.903	-0.848	-0.588
2.3	-0.659	-0.917	-0.855	-0.628
2.4	-0.621	-0.913	-0.863	-0.686
2.5	-0.515	-0.915	-0.872	-0.716
2.6	—	—	-0.897	-0.717
2.7	—	—	-0.928	-0.704
2.8	—	—	-0.930	-0.682
2.9	—	—	-0.923	-0.675
3.0	—	—	-0.921	-0.689
3.1	—	—	-0.919	-0.726
3.2	—	—	-0.914	-0.774
3.3	—	—	-0.908	-0.788
3.4	—	—	-0.901	-0.772
3.5	—	—	-0.910	-0.748
3.6	—	—	-0.952	-0.721
3.7	—	—	-0.986	-0.691
3.8	—	—	-0.990	-0.671
3.9	—	—	-0.960	-0.670
4.0	—	—	-0.891	-0.683

Table 3: K -corrections in the B, V, R (Johnson) and Gr (Gunn) bandpasses as derived from our composite spectrum.

It is to notice that for $z < 1$ there is a good agreement between our k -corrections and the ones derived from a spectrum with a constant slope $\alpha_\nu = -0.3$, whereas the difference rises to about 0.2 magnitudes at $z \sim 2$. This suggests that the hypothesis of a flat single-power-law spectrum leads to an underestimate of the luminosity of the QSO at high redshifts. Our results are in better agreement with the k -correction computed by Cristiani & Vio (1990) although in this case lower luminosities are predicted at $z < 2$ by our curve.

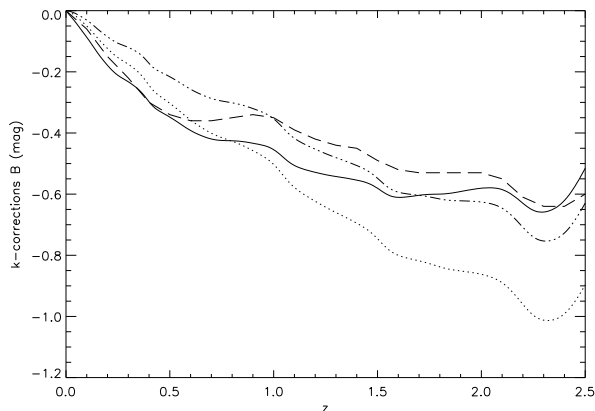


Fig. 5.— K -corrections in the B bandpass calculated in the case of our synthetic spectrum (*solid*) and spectra having single power-law continuum with spectral indexes -0.3 (*dotted*) and -0.5 (*dot-dashed*) compared with k -corrections given by Cristiani & Vio (1990) (*dashed*).

This new k -correction was used to estimate, by a maximum likelihood method, the optical luminosity function $\Phi(M_B, z)$ for a large sample of ~ 1000 QSOs, taken from various surveys in the literature as described in La Franca & Cristiani (1997). A double power law luminosity function and a pure luminosity evolution (PLE) model of the type (see La Franca & Cristiani 1997 for details):

$$\Phi(M_B, z) = \frac{\Phi^*}{10^{0.4[M_B - M_B^*(z)](\alpha+1)} + 10^{0.4[M_B - M_B^*(z)](\beta+1)}} \quad (3)$$

were assumed, where α and β are the slopes of the faint-end and bright-end luminosity function, respectively. $\Phi(M_B, z)$ is in units of $\text{Mpc}^{-3}\text{mag}^{-1}$. In this model the evolution is specified by the redshift dependence of the break magnitude ($M_B^*(z) = M_B^* - 2.5k \log(1+z)$), where $M_B^* \equiv M_B^*(z=0)$. This relationship corresponds to a power law evolution of the luminosity:

$$L^*(z) = L^*(1+z)^\kappa \quad (4)$$

The results are shown in Table 4 and Figure 6. The luminosity function computed using our k -correction has a value of the faint-end slope α between the values of the faint-end slope derived from the single power-law spectra, while the bright-end slope β is the same (within the errors). Moreover, the $z = 0$ break luminosity ($M_B^* \simeq -22.5$) does not change substantially with respect to the LF computed with the assumption of a single power-law slope, but the parameter κ , which gives the rate of the cosmological evolution, goes from the value 2.90 for a spectral index -0.3 to 3.12 for our spectrum, and the probability of the fit improves noticeably (Table 4).

Comparing our luminosity function with that computed by La Franca & Cristiani (1997) using the Cristiani & Vio (1990) k -correction we confirm the flattening at low redshift of the bright part of the luminosity function in comparison with a Pure Luminosity Evolution model. This is indicated by the poor fitting probabilities given by the two dimensional Kolmogorov-Smirnov test in the range ($0.3 \leq z \leq 0.6$) (see Table 4). However, the larger differences between our and Cristiani & Vio (1990) k -correction are at $z \sim 2$, where the discrepancy is of 0.2 magnitudes. This is at the origin of a evolutionary parameter which is about 2σ lower, resulting in a volume density of QSOs at $z \sim 2$ which is lower by a factor about 1.5 at $M_B \sim -27.5$.

Our more accurate estimates of the dispersions of the average spectral index as a function of wavelength ($\sigma = 0.3 - 0.4$ from Table 1) can also be included in the evaluation of the evolution of the luminosity function. Uncertainties in the estimate of the average spectral slopes are known to produce a smaller cosmological evolution of the luminosity function (Giallongo & Vagnetti 1992). In this case a value for the evolutionary parameter as small as $k = 2.94$ has been found (see Table 4). The probability of the PLE evolutionary models with the new k -corrections are in

spectrum model		κ	β	α	M^* $mag^{-1} Mpc^{-3}$	Φ^* $(z < 2.2)$	$P(\chi^2)$ $(0.3 < z < 0.6)$	$P(K-S)$
$\alpha_\nu = -0.3$	(a)	2.90	-3.79	-1.51	-22.5	8.9×10^{-7}	0.18	0.007
$\alpha_\nu = -0.5$	(a)	2.97	-3.84	-1.74	-22.9	5.6×10^{-7}	0.30	0.017
Cristiani & Vio (1990)	(a)	3.26	-3.72	-1.39	-22.3	1.1×10^{-6}	0.21	0.02
$\alpha_\nu = 1.5(\frac{\lambda}{4400}) - 1.5$	(a)	3.12	-3.73	-1.44	-22.4	9.6×10^{-7}	0.56	0.013
$\alpha_\nu = 1.5(\frac{\lambda}{4400}) - 1.5$	(b)	2.94	-3.84	-1.47	-22.4	1.0×10^{-6}	0.30	0.005
1σ errors		± 0.07	± 0.13	± 0.07	± 0.2			

Table 4: Parameters for luminosity function with different continuum shapes: (a) PLE model ($q_0 = 0.5$); (b) PLE model including a dispersion in the distribution of the spectral slope $\sigma = 0.4$ ($q_0 = 0.5$). The last two columns are respectively the χ^2 test probability and the two-dimensional Kolmogorov-Smirnov test probability (see details in La Franca & Cristiani, 1997).

general higher than previously found ($P(\chi^2) \sim 0.5$), showing how the selection of a more accurate average spectral shape can discriminate between different evolutionary models for the QSO luminosity function. In particular, there is no evidence for any redshift cutoff in the redshift evolution of the luminosity function as introduced by Boyle (1992) at $z = 1.9$.

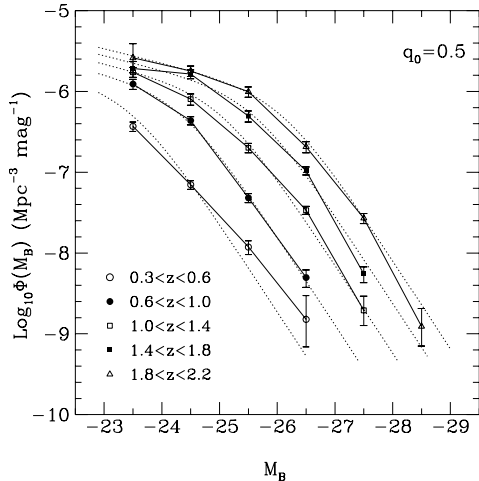


Fig. 6.— The QSO luminosity function. The points connected with a continuous line represent the observations (see La Franca & Cristiani, 1997 for details); the dotted lines are the best-fitting Pure Luminosity Evolution model. Error bars correspond to 1σ confidence intervals.

4.3. Modelling the emission mechanism

As an example of the consequences that more extended works of this type can have in constraining thermal emission models for the QSO continuum, we have compared with thermal models based on the presence of an accretion disk around a massive Kerr black hole ($10^6 - 10^9 M_\odot$) (Czerny & Elvis 1987). These models have been already used to fit the continua of QSOs in a wide wavelength interval extending to the X-ray band (Fiore et al. 1995).

The emission comes from a geometrically thin accretion disk around a massive black hole with accretion rates \dot{m} ranging in the sub-Eddington regime. For accretion rates much higher than the Eddington one the disks become slim and additional cooling processes should be included. In this illustrative example only sub-Eddington thin disks are considered.

The average shape has been normalized to $M_B \sim -24$ since higher luminosities require emission in a super-Eddington regime which is not allowed by the model. A qualitative comparison seems to indicate that only models with a large black hole mass ($M \simeq 10^{9.5} M_\odot$), an average inclination along the line of sight $\mu = \cos\theta = 0.5$ with an intermediate accretion rates $\dot{m} = 0.3$, or smaller inclination ($\mu = \cos\theta = 0.75$) and higher accretion rate ($\dot{m} = 0.8$) can reproduce a change of slope $\Delta\alpha \approx 1$ at $\bar{\lambda} \approx 3200 \text{ \AA}$ (Figure 7). Models with smaller black hole masses ($M \leq 10^{7.5} M_\odot$) provide much lower luminosities, while models with masses between $10^8 M_\odot$ and $10^{8.5} M_\odot$ present a softer continuum shape than the observed one. For black hole masses $M \approx 10^9 -$

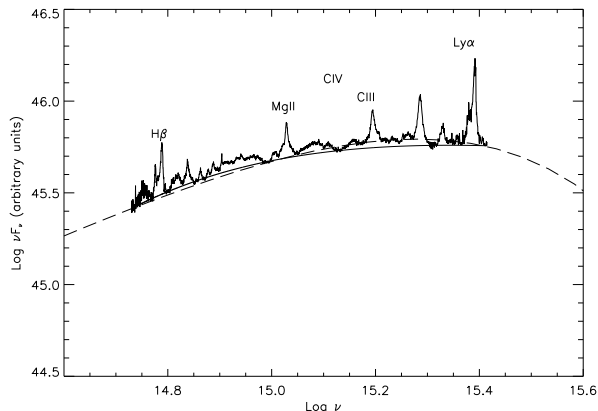


Fig. 7.— Composite spectrum with the continuum component (*solid*), as estimated in the present work, compared to the synthetic continuum spectrum derived from thermal emission models of an accretion disk around a massive Kerr’s black hole. The best fitting model ($M = 10^{9.5}M_{\odot}$, $\dot{m} = 0.8$ and $\cos\theta = 0.75$; see Fiore et al., 1995, for details) is shown (*dashed*).

$10^{9.5}M_{\odot}$, high accretion rates, and smallest inclination angles ($\cos\theta = 1$ corresponds to a face-on disk) there is a good agreement for $\text{Log}\nu \leq 15.2$, but the large masses involved in the accretion process produce a drop of the luminosity in the blue part of the spectrum.

5. Conclusion

In this paper we have analysed the spectra of 62 QSOs in the magnitude interval $B = 15 - 20$ having good relative photometric calibrations. The analysis was performed fitting power-law continua $f_{\nu} \propto \nu^{\alpha}$ in well defined rest-frame wavelength intervals after removing regions of the spectrum affected by strong emission lines or weak emission bumps.

The main results of the paper can be summarized as follows:

- The mean values of the continuum slopes obtained in the spectra of 62 QSOs change from $\alpha \sim 0.15$ at $\lambda > 3000 \text{ \AA}$ to $\alpha \sim -0.65$ at $\lambda < 3000 \text{ \AA}$.
- Assuming a linear change of the local slope with the rest-frame wavelength we obtain the following relation $\alpha = 1.5(\lambda/4400) - 1.5$

- There is no correlation in the sample between α and redshift and/or luminosity.
- New k -corrections, which include the contribution of emission features, are derived for the B, V, R (Johnson) and Gr (Gunn) bands.
- The new k -corrections are used to estimate the evolution of the QSO luminosity function. Assuming PLE models, the double power-law luminosity function evolves as $L \propto (1+z)^{3.1}$ or as low as $L \propto (1+z)^{2.9}$ if we take into account the dispersion in the distribution of spectral shapes.
- A qualitative comparison of the QSO average continuum shape with thermal models based on the presence of a thin accretion disk around a massive Kerr black hole seems to indicate that only models with a large black hole mass ($M \simeq 10^{9.5}M_{\odot}$) can reproduce a change of slope $\Delta\alpha \approx 1$ at $\bar{\lambda} \approx 3200 \text{ \AA}$.

The authors acknowledge B. Czerny and A. Siemigowska for the code of the accretion disk model and F. Fiore for useful discussions. We warmly thank the referee P. Francis for his suggestions. This research has made use of the Simbad database, operated at CDS, Strasbourg, France.

REFERENCES

- Baldwin, J. A., Wampler, W. J. & Gaskell, C. M. 1989 ApJ, 338, 630
- Banase, K., Crane, P., Ounnas, C. & Ponz, D. 1983 In: *Proc. of DECUS*, Zurich, p. 87
- Barvainis, R. 1993, ApJ, 412, 513
- Boyle, B. J. 1992 in “Texas/ESO-CERN Symposium on Relativistic Astrophysics, Cosmology and Particle Physics”, ed(s) Barrow et al., Ann. N.Y. Acad. of Sci., 647, 14
- Boyle, B. J., Shanks, T. & Peterson, B. A. 1988, MNRAS, 235, 935
- Cheng, F. H., Gaskell, C. M. & Koratkar, A. P. 1991, ApJ, 370, 487
- Cristiani, S., La Franca, F., Andreani, P., Gemmo, A., Goldschmidt, P., Miller, L., Vio, R., Barbieri, C., Bodini, L., Iovino, A., Lazzarin, M., Clowes, R.,

- MacGillivray, H., Gouiffes, Ch., Lissandrini, C. & Savage, A. 1995, *A&AS*, 112, 347
- Cristiani, S., Trentini, S., La Franca, F., Aretxaga, I., Andreani, P., Vio, R., & Gemmo, A. 1996, *A&A*, 306, 395
- Cristiani, S., & Vio, R. 1990, *A&A*, 227, 385
- Czerny, B., & Elvis, M. 1987, *ApJ*, 321, 305
- Elvis, M., Wilkes, B. J., McDowell, J. C., Green, R. F., Bechtold, J., Willner, S. P., Oey, M. S., Polomsky, E., & Cutri, R. 1994, *ApJS*, 95, 1
- Fasano, G. & Vio, R. 1988, "Newsletter of the Working Group for Modern Astronomical Methodology" 7, 2
- Fiore, F., Elvis, M., Siemiginowska, A., Wilkes, B. J., McDowell, J. C., & Mathur, S. 1995, *ApJ*, 449, 74
- Francis, P. J., Hewett, P. C., Foltz, C. B., Chaffee, F. H., Weymann, R. J., & Morris, S. L. 1991, *ApJ*, 373, 465
- Francis, P. J. 1993, *ApJ*, 407, 519
- Francis, P. J. 1996, *PASA*, 13, 212
- Giallongo, E., & Vagnetti, F. 1992, *ApJ*, 396, 411
- La Franca, F., Cristiani, S., & Barbieri, C. 1992, *AJ*, 103, 1062
- La Franca, F., & Cristiani, S. 1997, *AJ*, 113, 1517
- O'Brien, P. T., Gondhalekar, P. M., & Wilson, R. 1988, *MNRAS*, 233, 801
- Oke, J. B. 1974, *ApJS*, 27, 21
- Oke, J. B., & Korycansky, D. G. 1982, *ApJ*, 255, 11
- Oke, J. B., Shields, G. A., & Korycansky, D. G. 1984, *ApJ*, 277, 64
- Richstone, D. O., & Schmidt, M. 1980, *ApJ*, 235, 361
- Sanders, D. B., Phinney, E. S., Neugebauer, G., Soifer, B. T., & Matthews, K. 1989, *ApJ*, 347, 29
- Sargent, W. L. W., Steidel, C. C., & Boksenberg, A. 1989, *ApJS*, 69, 703
- Serjeant, S., & Rawlings, S. 1996, *Nature*, 379, 304
- Stone, R. P. S. 1977, *ApJ*, 218, 767
- Webster, R. L., Francis, P. J., Peterson, B. A., Drinkwater, M. J., & Masci, F. J. 1995, *Nature*, 375, 469